Metal Nanoparticle Based All-Optical Photothermal Light Modulator

André Heber, Markus Selmke, and Frank Cichos*

Molecular Nanophotonics Group, Institute of Experimental Physics I, Universität Leipzig, 04103 Leipzig, Germany

ABSTRACT We present a simple scheme for the manipulation of light intensity by light mediated by a dissipative process. The implementation employs the heat released by an optically excited plasmonic metal nanoparticle to control the size of an isotropic bubble in a nematic liquid crystal film. The nematic film is designed as a zero-order half-wave plate that rotates an incident probe light polarization by $\pi/2$ and is blocked by an analyzing polarizer behind the structure. The growing isotropic bubble disturbs the half-wave plate and causes the probe to be transmitted through the modulator structure. Our results demonstrate that dissipative processes may be advantageously used to control light by light.

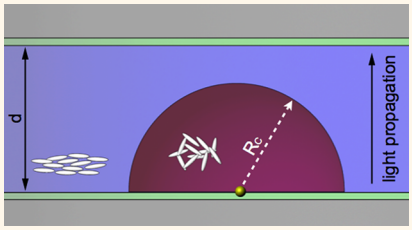

KEYWORDS: all-optical modulation · liquid crystals · gold nanoparticle · phase transition · photothermal effects · absorption

Controlling light propagation with light is intrinsically difficult as the photon−photon interaction cross sections are almost vanishing.[1] Thus dielectric media have to pick up the role of photonic modulators, and a number of different and highly advanced schemes have been proposed to control the flow of light by light with the help of nonlinear optical effects,[2,3] optical resonators,[4] exciton polaritons,[5,6] or with the optical response of a two-level system in a single fluorescent molecule.[7] Approaches utilizing photoexcited carriers in biased p-i-n diodes provide high speed switching at GHz frequencies.[8] Twisted liquid crystal cells allow for polarization control in light propagation.[9] Many of these schemes utilize highly advanced structures and technologies for realizing these photonic modulators. Here, we report on an extremely simple all-optical modulator based on a single metal nanoparticle embedded in a liquid crystal. The transmission of a focused laser beam is controlled by the local phase composition in a liquid crystalline cell. This phase composition is varied by an optical signal heating a gold nanoparticle. The presented modulator can be easily prepared by simple self-organization methods and provides an example of a slow-speed dissipative switch to control the propagation of light by light.

Our all-optical intensity modulator is constructed as a zero-order half-wave plate (see Figure 1 and Materials and Methods section). Therefore, we utilize a homogeneously aligned liquid crystal layer with accurately tuned thickness into which single gold nanoparticles are embedded.

The birefringence of the liquid crystal causes a phase retardation β (eq 1) between the electric field components parallel and perpendicular to the director according to the ordinary n_o and extraordinary refractive index n_e,[10] the thickness d of the liquid crystal film, and the vacuum wavelength λ_d of the incident probe laser beam:

$$\beta = \frac{2\pi(n_e - n_o)d}{\lambda_d} \qquad (1)$$

This retardation β increases with the thickness d at a given refractive index contrast $\Delta n = n_e - n_o$, which is specified by the choice of the liquid crystal. At a retardation of $\beta = \pi$ the liquid crystalline layer acts as a half-wave plate. This is fulfilled for $d = d_{min} =$ 3.2 μm thick 5CB layer at $T = 307$ K.[10] At this thickness, the liquid crystal acts as a zero-order half-wave-plate rotating an incident polarization of $\Theta = \pi/4$ by $\pi/2$, where Θ is the polarization angle with respect to the liquid crystal director.

As the transmitted light impinges on the analyzer oriented parallel to the incident polarization, no light is transmitted through the modulator structure. The transmission through the whole structure including the

* Address correspondence to cichos@physik.uni-leipzig.de.

Received for review December 13, 2013 and accepted January 17, 2014.

Published online January 17, 2014
10.1021/nn406389f

two polarizers then follows as[11]

$$\mathcal{T} = \frac{I(\beta,\Theta)}{I_0} = 1 - \sin^2(2\Theta)\sin^2(\beta/2) \qquad (2)$$

An intensity modulator based on a nematic liquid crystal film thus has to control the thickness of the nematic phase optically. This can be achieved by a gold nanoparticle placed on the PVA/5CB interface. While the gold nanoparticle itself may induce a local distortion of the director structure,[12] it only negligibly perturbs the local transmission through the cell. If the gold nanoparticle, however, is placed in the focus of a laser beam resonant to the wavelength of the plasmon resonance (λ_h = 532 nm), the heat released by the particle[13] will cause a local phase transition from the nematic to the isotropic phase. The hot nanoparticle therefore generates an isotropic bubble, which decreases the thickness of the nematic layer locally and thus causes a smaller retardation of the field components of a weakly absorbed laser wavelength λ_d (see Figure 1 for a sketch). If this isotropic bubble extends across the whole film thickness, all light is transmitted. Consequently, the optically controlled heat dissipation of the nanoparticle at its plasmon resonance controls the light transmitted through the modulator structure between 0 and 100%. As the liquid crystal is well-ordered on length scales of the probe beam waist, the total optical contrast is mainly related to the quality of the polarizers in the modulator structure.

RESULTS AND DISCUSSION

Stationary Response of the Modulator Structure. In the steady state the phase boundary between the nematic and the isotropic liquid crystalline phase occurs at a distance R_C, where the phase-transition temperature matches the local temperature $T(R_C) = T_C$. Since the liquid crystal structure is anisotropic, the heat conductivity is anisotropic as well, and the phase boundary is nonspherical.[14] Further the interface to the PVA film and to the glass cover slide will distort the temperature profile.[15] For simplicity, however, we model the temperature profile to be isotropic such that

$$\Delta T(r) = T(r) - T_0 = \frac{P_{abs}}{4\pi\kappa r} = \frac{1}{4\pi\kappa r}\frac{2\sigma_{abs}P_{inc}}{\pi\omega_h^2} \qquad (3)$$

with P_{abs} being the absorbed laser power at λ_h = 532 nm, T_0 the ambient temperature, κ the average thermal conductivity of the liquid crystal, P_{inc} the heating power incident on the back aperture of the microscope objective, $\sigma_{abs} = 9.6 \times 10^{-15}$ m^2 the gold nanoparticle absorption cross-section, and ω_h = 270 nm the beam waist of the heating laser. Taking all effects into account that lower the intensity incident on the particle, P_{inc} = 100 μW corresponds to P_{abs} = 2.6 μW (see also the Supporting Information). The changing radius of the isotropic bubble actually requires a detailed analysis of the light scattering properties of the isotropic bubble, which is beyond the simple demonstration targeted here. However, we note that a detailed modeling of the light scattering at this liquid crystal structure will allow a detailed study of local phase transitions in liquid crystals as well, which is a new and promising field of research for itself.[16,17]

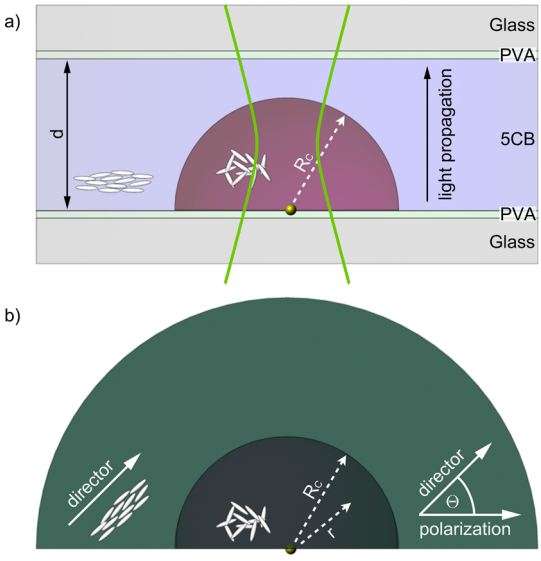

Figure 1. Scheme of the photothermal light modulator. (a) Side view: The modulator structure consists of a liquid crystal and a gold nanoparticle heated optically to convert the liquid crystal from the nematic to the isotropic phase. (b) Top view: The principle axis of the liquid crystal in the nematic phase is oriented at 45° to the polarization of the detection laser. The liquid crystal film of a well-defined thickness d_{min} forms a zero-order half-wave plate.

Here, we describe the change in the transmission by assuming that the thickness of the nematic phase is given by the overall film thickness d_{min} minus the radius R_C of the isotropic bubble created around the gold nanoparticle (see Figure 1). Under steady state conditions the radius of the isotropic bubble is given according to eq 3 by $R_C = R\Delta T/[T_C - T_0]$, where R is the particle radius and $\Delta T = \Delta T(R)$ the temperature increase on the surface of the particle induced by the optical heating. Thus the phase retardation is

$$\beta = \frac{2\pi\Delta n}{\lambda_d}\left[d_{min} - R\frac{\Delta T}{T_C - T_0}\right] \qquad (4)$$

and using eq 2 the transmission through the modulator structure for an incident polarization of $\Theta = \pi/4$ is found to be

$$\mathcal{T}(\Delta T, T_0) = \cos^2\left(\frac{\pi\Delta n}{\lambda_d}\left[d_{min} - R\frac{\Delta T}{T_C - T_0}\right]\right) \qquad (5)$$

According to eq 5, the transmission depends only on the particle radius R, the ambient temperature T_0, and the temperature increment ΔT at the particle surface. Figure 2 (inset) plots the expected transmission for various ambient temperatures as a function of the particle temperature rise. At ΔT = 0 the modulator structure shows zero transmission, while the transmission becomes maximal at $\Delta T = [T_C - T_0]d_{min}/R$. Thus the temperature

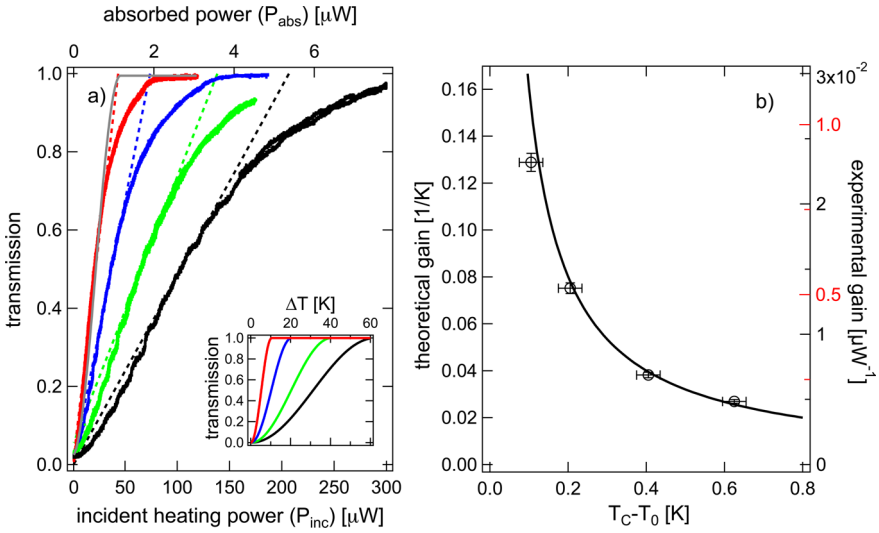

Figure 2. (a) Steady state response: The transmission of the probe laser beam is plotted against the incident heating power. It is varied sufficiently slowly to achieve a steady state transmission signal of the system at each incident heating power. The transmission is shown at different temperatures $T_C - T_0$ being 0.11 K (red), 0.21 K (blue), 0.43 K (green), and 0.63 K (black) below the nematic to isotropic phase-transition temperature T_C = 307.5 K. The corresponding dashed lines are tangents of the maximum slopes indicating the linear regime and determining the experimental gain. The gray line is a fit of eq 5 to the experimental data. The inset shows the theoretically derived transmission as a function of the temperature increase at the nanoparticle's surface according to eq 5. (b) Gain factors: Comparison of theoretical (line) and experimental gain factors (markers), which correspond to the maximum transmission increase per temperature and incident heating/absorbed power (see eq 7). The labels on the right axis correspond to the experimental gain with respect to P_{inc} (black) and P_{abs} (red).

rise required to switch from zero to full transmission decreases the closer the ambient temperature T_0 is to the phase-transition temperature. The corresponding absorbed heating power is

$$P_{abs}^{min} = 4\pi\kappa d_{min}(T_C - T_0) \quad (6)$$

Above this absorbed power, no further transmission changes occur. As the film thickness d_{min} is typically 100 times larger than the particle radius R and the ambient temperature is about 0.1 K below the phase-transition temperature, it requires a temperature rise of just 10 K to switch from 0 to 100% transmission. The calculated transmission curves displayed in Figure 2 (inset) also reveal that the slope of the transmission curve is controlled by the ambient temperature. Thus a small particle temperature variation $\delta\Delta T$ causes a strong transmission variation $\delta\mathcal{T}$ if the ambient temperature is close to the phase-transition temperature. The maximum slope of the transmission function $\mathcal{T}$ (eq 5) therefore defines the gain $\mathcal{G}$ (eq 7) of the system; *i.e.*, the maximum transmission factor change per Kelvin particle temperature rise at an ambient temperature T_0:

$$\mathcal{G} = \left.\frac{\delta\mathcal{T}}{\delta\Delta T}\right|_{\mathcal{T}=1/2} = \frac{\pi\Delta n}{(T_C - T_0)}\frac{R}{\lambda} \quad (7)$$

This gain factor diverges in case the ambient temperature corresponds to the phase-transition temperature $T_0 = T_C$. It decays to zero if the ambient temperature is far below the phase-transition temperature. The modulator structure therefore has two control parameters defining the transmission. The first is the heating power, which controls the particle temperature rise and thus corresponds to the base voltage of an electrical transistor, and second the ambient temperature, which controls the gain.

Experimental transmission data obtained with a 5CB liquid crystal modulator described above is displayed in Figure 2a. Details of the experimental setup can be found in the Supporting Information and in ref 16. The graph shows the transmission at various incident heating powers and different ambient temperatures, T_0. The ambient temperature is thereby controlled with a resistive heater attached to the objective. The experimental data clearly follow the predicted behavior. The closer the ambient temperature gets to the phase-transition temperature, the steeper is the increase in transmission with the incident heating power. The experimental data can be actually fitted with eq 5 displaying a good agreement. However, at low powers deviations occur, which are due to the fact that the isotropic bubble is smaller than the beam waist of the probe beam. Between 80 and 100%, the saturation of the transmission signal with rising incident heating power is slower than in the experiment because of the spherical shape of the nematic to isotropic interface. The maximum slope of the curve is shown in Figure 2b, characterizing the amplification factor of the modulator structure. The experimental gain factor $\mathcal{G}$ is given by the maximum slope on the transmission curve with increasing heating power. The incident heating power can be converted into a particle temperature rise using the absorbed fraction of the power (see Supporting Information). This absorbed

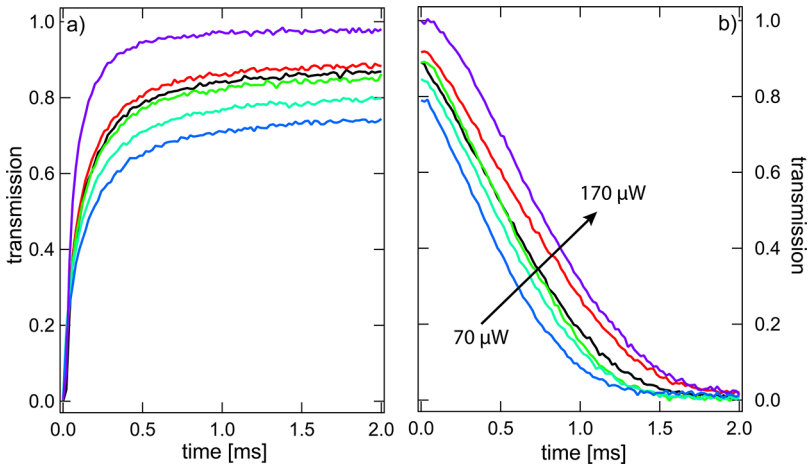

Figure 3. Step response of the optical modulator at $T_C - T_0 = 0.2$ K: The transmission of the modulator structure is displayed in response to a step-like switching of the heating laser. (a) The switch-on response is plotted for incident heating powers at 70 (blue), 85 (light blue), 95 (green), 103 (black), 123 (red), and 170 μW (violet). (b) Switch-off response of the modulator structure at the same incident heating powers as in (a).

fraction of the heating power is given by the fraction of the absorption cross-section σ_{abs} compared to the illuminated focus area with a radius of 270 nm (see eq 3). Accordingly, a power of 10 μW incident heating power corresponds to a temperature increase of about 1 K. Experimental gain values are given in μW^{-1}, since the temperature of the particle is not exactly known. The theoretical data is included using the left axis for a gold nanoparticle with $R = 30$ nm in a 5CB environment. Both the experimental and theoretical gain factor agree well in their dependence on the ambient temperature T_0. Thus, when stabilizing the ambient temperature very close to the nematic−isotropic phase-transition temperature, strong changes of the transmitted optical power can be obtained for very small changes in the incident optical control beam. This is in contrast to most all-optical modulators demonstrated before, which control a weak signal with a very intense control beam. In the case of the presented photothermal modulator, this probe power is only limited by the absorption of the probe power by the gold nanoparticle.

Dynamic Response of the Modulator Structure. The second key factor characterizing the modulator is related to the dynamics of the switching process. Here, the switching from zero transmission to the steady state transmission and back is studied as a function of the incident heating power. Therefore, the probe laser beam is focused onto the particle, the heating laser beam is switched on/off, and the time-dependent probe response is recorded at a time resolution of 20 μs. At 0.2 K below the phase-transition temperature, 50% of the transmission is reached after 0.1 ms. The experimental data are shown in Figure 3 for six different heating powers and reveal that most of the signal change is occurring within a few milliseconds.

To quantify the time scale, we plot the time when half the steady state signal is reached in either the switch-on or the switch-off process (see Figure 4a). As found, the switch-on time is about 100 μs and almost constant for the considered heating power range. The switch-off time, however, increases with increasing heating power. This can be qualitatively understood from the following arguments. We assume, that the time required to reach half the steady state signal is mainly determined by the latent heat required to convert the liquid crystal from the nematic to the isotropic phase in volume $V_{1/2}$.[18] The radius of the isotropic bubble grows linearly with the absorbed heating power. The radius $R_{1/2}$ of the isotropic bubble required to generate half the steady state signal, however, does not increase linearly with the heating power, since the relation between heating power and signal is nonlinear (see Figure 2 (inset)). $R_{1/2}$ saturates for heating powers close to maximum transmission, which means that the volume to be converted to the isotropic phase in the switch-on process is almost constant at larger heating powers. The studied steady state transmission range between 0.7 and 1 corresponds to this large heating power regime, and thus no dependence of the switch-on time on the heating power is observed.

In the switch-off case, however, the initial isotropic volume before switching the heating power off is still a linear function of the heating power. The signal drops from the stationary isotropic bubble radius to the half-signal radius $R_{1/2}$. Thus the time scale of the switch-off is still increasing with increasing heating power. The estimated time scales for the switch-on and switch-off process based on these considerations (see the Supporting Information for a detailed calculation) are plotted in Figure 4a, scaled in y-direction, and confirm the observed trend. The switch-on and switch-off times differ as different processes are responsible for their time scale. The switch-on time depends on the rate at which the latent heat of the phase transition is supplied to the liquid crystal by the incident laser radiation, whereas the switch-off time results from the transport of the latent to the environment and thereby on the thermal diffusivity.

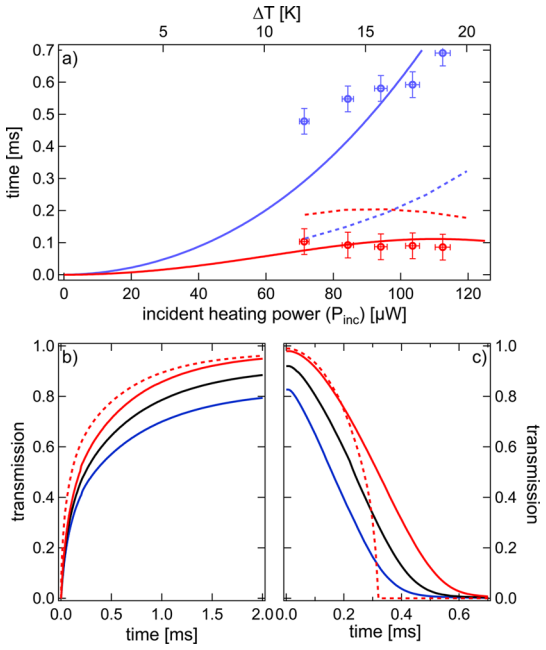

Figure 4. Comparison of experimental and theoretical switching times at $T_C - T_0 = 0.2$ K: (a) The times required to change the transmission signal of the modulator by 50% are plotted for the switch-on (red) and switch-off process (blue). The dashed lines show the results of the numerical simulations. The solid lines represent the trend from a simple analytical model (see Supporting Information). The markers display the experimental results. (b) and (c) show the corresponding time-dependent transmission signals obtained from the simulations using eq 8 to get steady state transmission at $\mathcal{T} = 83\%$ (blue), $\mathcal{T} = 92\%$ (black), and $\mathcal{T} = 100\%$ (red). The solid lines include a heating effect due to the detection laser, whereas the red dashed line excludes that effect.

A more quantitative analysis requires considering the time-dependent heat equation including the phase transition. The dynamics of a liquid crystal phase transition involving a moving phase boundary can only be solved numerically. For this purpose we employ the apparent heat capacity method.[19] This method introduces an apparent heat capacity at the phase boundary consisting of the heat capacity C of the liquid crystal and the latent heat H_f of the nematic to isotropic phase transition. We assume a spherically symmetric system neglecting the presence of the PVA/glass interfaces and the anisotropic thermal conductivity κ, which allows transforming the apparent heat capacity equation into spherical coordinates

$$\rho\left(C\frac{\partial T}{\partial t} + H_f\delta(T - T_C)\right) = \frac{1}{r^2}\frac{\partial}{\partial r}\left(\kappa r^2\frac{\partial T}{\partial r}\right) + S \quad (8)$$

with ρ being the mass density and $\delta(T - T_C)$ the delta distribution. The term S represents a heat source present in form of the gold nanoparticle. To be as close as possible to the experimental conditions, we include a steady heating effect caused by the probe laser in the source as well. Using the corresponding boundary conditions, we obtain the transient temperature profile in the liquid crystal numerically (see the Supporting Information). To obtain the optical signal from the temperature profile, we extract the radius of the phase boundary and employ eq 5. The results of the numerical calculation are shown in Figure 4b,c for switch-on and -off process. The shown striking similarity to the experimental results further reveals the correct trends with increasing heating power (see Figure 4a). However, the absolute time scale deviates by a factor of 2. We suppose that this deviation results from the influence of the probe laser heating the particle. Neglecting the influence of the probe laser in the simulations reveals a steeper response in the switch-on and the switch-off process as depicted by the dotted lines in Figure 4b,c. Thus the probe laser may play an important role for the dynamics of the optical switching process in the modulator structure. The deviations between experimental and numerical data result from the simplifications made to solve the time-dependent heat conduction equation including a moving phase boundary and to model the light propagation. Two of the assumptions are plane wave propagation for the optical signal and a spherical geometry of the phase boundary in the heat conduction model. A technically more defined model will therefore lead to quantitative agreement. The major physics, however, is already captured by the simplified theory presented above.

CONCLUSION

We have presented a simple all-optical modulator based on an absorbing nanoparticle dissipating its excitation energy as heat. We use an inherently linear process, the absorption of a single absorbing nanoparticle, to modulate the transmission of a second beam of light using a driven phase transition of a liquid crystal. While the speed of the modulating structure is limited by the phase transition, the main goal of this report is to demonstrate that dissipative optical processes may provide a scheme to manipulate light as well. The performance of the device could easily be improved by using nanoparticles with a sharper and larger surface plasmon resonance like gold nanorods. Faster structures using Mach–Zehnder type interferometers where the optical phase in one interferometer arm is manipulated by optically controlled heating may speed up light modulation considerably.

MATERIALS AND METHODS

Single gold nanoparticles ($R = 30$ nm) are immobilized in a thin polymer film (about 20 nm, polyvinyl alcohol, PVA) on a glass cover slide. The resulting film is rubbed by a lens cleaning tissue to align the director of a nematic liquid crystal deposited on top of the polymer film.[20] The whole structure is covered by a second cover glass slide also coated with a rubbed PVA layer. The rubbing directions of both sides are aligned parallel to ensure a homogeneous, untwisted alignment of the liquid crystal director throughout the sample. The modulator structure

is assembled utilizing a spacer on one side of the sample to cause a film thickness variation across the sample with thickness values between 1 and 10 μm. The resulting space between the two glass cover slides is filled with 2 μL of the liquid crystal 5CB (4-cyano-4′-pentylbiphenyl) by capillary forces. This liquid crystal cell is placed between two parallel polarizers (a polarizer and an analyzer). A polarization contrast image of the sample structure at a wavelength of λ_d = 635 nm reveals the homogeneous alignment of the liquid crystal molecules[11] (see the Supporting Information).

Conflict of Interest: The authors declare no competing financial interest.

Acknowledgment. We acknowledge financial support from the European Union, the Free State of Saxony, and the DFG Forschergruppe "From Local Constraints to Macroscopic Transport".

Supporting Information Available: A detailed description on the characterization of the sample, the experimental setup, and the analytical model as well as further details on the numerical calculations. This material is available free of charge *via* the Internet at http://pubs.acs.org.

REFERENCES AND NOTES

1. Marklund, M.; Lundin, J. Quantum Vacuum Experiments Using High Intensity Lasers. *Eur. Phys. J. D* **2009**, *55*, 319–326.
2. Pacifici, D.; Lezec, H. J.; Atwater, H. A. All-Optical Modulation by Plasmonic Excitation of CdSe Quantum Dots. *Nat. Photonics* **2007**, *1*, 402–406.
3. Min, C.; Wang, P.; Chen, C.; Deng, Y.; Lu, Y.; Ming, H.; Ning, T.; Zhou, Y.; Yang, G. All-Optical Switching in Subwavelength Metallic Grating Structure Containing Nonlinear Optical Materials. *Opt. Lett.* **2008**, *33*, 869–871.
4. Almeida, V. R.; Barrios, C. A.; Panepucci, R. R.; Lipson, M. All-Optical Control of Light in a Silicon Chip. *Nature* **2004**, *431*, 1081–1084.
5. Gao, T.; Eldridge, P. S.; Liew, T. C. H.; Tsintzos, S. I.; Stavrinidis, G.; Deligeorgis, G.; Hatzopoulos, Z.; Savvidis, P. G. Polariton Condensate Transistor Switch. *Phys. Rev. B: Condens. Matter Mater. Phys.* **2012**, *85*, 235102.
6. Ballarini, D.; De Giorgi, M.; Cancellieri, E.; Houdré, R.; Giacobino, E.; Cingolani, R.; Bramati, A.; Gigli, G.; Sanvitto, D. All-Optical Polariton Transistor. *Nat. Commun.* **2013**, *4*, 1778.
7. Hwang, J.; Pototschnig, M.; Lettow, R.; Zumofen, G.; Renn, A.; Götzinger, S.; Sandoghdar, V. A Single-Molecule Optical Transistor. *Nature* **2009**, *460*, 76–80.
8. Preble, S. F.; Xu, Q.; Schmidt, B. S.; Lipson, M. Ultrafast All-Optical Modulation on a Silicon Chip. *Opt. Lett.* **2005**, *30*, 2891–2893.
9. Khoo, I.-C. *Liquid Crystals*; John Wiley & Sons, Inc.: Hoboken, NJ, USA, 2007.
10. Horn, R. G. Refractive Indices and Order Parameters of two Liquid Crystals. *J. Phys. (Paris)* **1978**, *39*, 105–109.
11. Durán, V.; Lancis, J.; Tajahuerce, E.; Jaroszewicz, Z. Cell Parameter Determination of a Twisted-Nematic Liquid Crystal Display by Single Wavelength Polarimetry. *J. Appl. Phys.* **2005**, *97*, 043101.
12. Shan, J.; Shi, W.; Liu, L. Y.; Shen, Y. R.; Xu, L. Optical Control of Surface Anchoring and Reorientation of Liquid Crystals *via* a Plasmon-Enhanced Local Field. *Phys. Rev. Lett.* **2012**, *109*, 147801.
13. Zijlstra, P.; Orrit, M. Single Metal Nanoparticles: Optical Detection, Spectroscopy and Applications. *Rep. Prog. Phys.* **2011**, *74*, 106401.
14. Marinelli, M.; Mercuri, F.; Zammit, U.; Scudieri, F. Thermal Conductivity and Thermal Diffusivity of the Cyanobiphenyl (nCB) Homologous Series. *Phys. Rev. E: Stat. Phys., Plasmas, Fluids, Relat. Interdiscip. Top.* **1998**, *58*, 5860–5866.
15. Baffou, G.; Quidant, R.; Girard, C. Thermoplasmonics Modeling: A Green's Function Approach. *Phys. Rev. B: Condens. Matter Mater. Phys.* **2010**, *82*, 165424.
16. Selmke, M.; Braun, M.; Cichos, F. Photothermal Single-Particle Microscopy: Detection of a Nanolens. *ACS Nano* **2012**, *6*, 2741–2749.
17. Selmke, M.; Braun, M.; Cichos, F. Nano-Lens Diffraction Around a Single Heated Nano Particle. *Opt. Express* **2012**, *20*, 8055–8070.
18. Govorov, A. O.; Zhang, W.; Skeini, T.; Richardson, H.; Lee, J.; Kotov, N. A. Gold Nanoparticle Ensembles as Heaters and Actuators: Melting and Collective Plasmon Resonances. *Nanoscale Res. Lett.* **2006**, *1*, 84–90.
19. Hu, H.; Argyropoulus, S. A. Mathematical Modelling of Solidification and Melting: a Review. *Modell. Simul. Mater. Sci. Eng.* **1996**, *4*, 371–396.
20. Ishihara, S. How Far Has the Molecular Alignment of Liquid Crystals Been Elucidated? *J. Disp. Technol.* **2005**, *1*, 30–40.